Japanese Journal of Gastroenterology and Hepatology

Clinical Report

ISSN: 2435-1210 | Volume 8

Application of Diffusion Kurtosis Imaging in Predicting the Recurrence and Postoperative Liver Function Deterioration of Hepatocellular Carcinoma after Transarterial Chemoembolization Treatment

Cai M[1], Jia F[1], Yan R[2], Li X[2], Ren J[2], Wang K[2] and Han D[1*]

[1]Department of MR, The First Affiliated Hospital, Xinxiang Medical University, Weihui, China,

[2]MR Research China, GE Healthcare, Beijing, China

***Corresponding author:**

Dongming Han,
Department of MR, The First Affiliated Hospital, Xinxiang Medical University, Weihui, China, E-mail: 625492590@qq.com

Received: 12 Jan 2022
Accepted: 21 Jan 2022
Published: 28 Jan 2022
J Short Name: JJGH

Citation:

Han D, Application of Diffusion Kurtosis Imaging in Predicting the Recurrence and Postoperative Liver Function Deterioration of Hepatocellular Carcinoma after Transarterial Chemoembolization Treatment. Japanese J Gstro Hepato. 2022; V8(3): 1-9

Keywords:

Hepatocellular carcinoma, Transarterial chemoembolization, Diffusion kurtosis Imaging, recurrence, Liver function deterioration

1. Abstract

1.1. Background and Aim: This study is to investigate the value of Diffusion Kurtosis Imaging (DKI) in predicting the recurrence and postoperative liver function deterioration of intermediate-stage hepatocellular carcinoma treated with Transarterial Chemoembolization (TACE).

1.2. Methods: Sixty-three patients with HCC in this study were divided into recurrence (n = 33) and non-recurrence (n = 30) groups after a follow-up of 6 months. And the 30 recurrence patients were divided into liver function deterioration (n = 7) and non-deterioration groups (n = 26). Preoperative parameters derived from DKI includes Mean Diffusivity (MD), Mean Kurtosis (MK) and Fractional Anisotropy (FA). Univariate and multivariate logistic Regression and Operating Characteristic (ROC) curve were used for statistical analyses.

1.3. Results: The MK values of the tumor and peritumoral tissues were significantly higher in the recurrence group than in the non-recurrence group, while the MD value of the tumor tissue was lower in recurrence group. The MK value of the normal tissues was higher in the liver function deterioration group than in the non-deterioration group, while the MD value was lower in the liver function deterioration group. The parameter MK and the tumor size were the independent predictors for the recurrence treated with TACE. The AUC for predicting recurrence was 0.861. For the liver function deterioration, only the parameter MK was the independent predictor with a diagnostic efficiency of 0.832.

1.4. Conclusion: DKI has the potential to predict the effect of intermediate-stage HCC after TACE treatment.

2. Introduction

Hepatocellular Carcinoma (HCC) is the most common primary liver malignancy and the second leading cause of death in the world. Most of the patients have lost their surgical evidence on admission, and Transarterial Chemoembolization (TACE) is the first choice for non-surgical treatment for primary liver cancer [1]. However, TACE treatment can aggravate the damage of liver function and lead to liver function deterioration, and some patients are prone to early recurrence due to tumor angiogenesis. Moreover, study has shown that there are differences in survival rates among patients treated with TACE, which may be related to differences in liver function and tumor burden among patients at the same disease stage [2]. In addition, for patients with TACE refractoriness, switching to another treatment would not be a problem if liver function does not deteriorate. Accurate prediction of liver reserve function in patients with HCC is helpful to evaluate the prognosis of patients. Therefore, it is very important to quickly and accurately predict the postoperative treatment response and liver function deterioration.

In recent years, many studies have shown that liver cancer is highly heterogeneous. The tumor is not only composed of tumor cells, but

also includes the complex microenvironment around the tumor [3]. Tumor microenvironment is a key factor in tumor development and therapeutic response [4]. Magnetic Resonance Imaging (MRI) can provide multi-quantitative and multi-parameter imaging, with high soft tissue contrast and spatial resolution, and does not produce serious complications during routine follow-up for residual detection and recurrence of hepatocellular carcinoma after TACE. Studies have shown that Contrast-Enhanced Magnetic Resonance Imaging (CEMRI) [5-7] is a well-established imaging method for detecting residual or recurrent hepatocellular carcinoma, gadoxetic acid-enhanced magnetic resonance imaging (GA-MRI) [8-11] have been used to evaluate of treatment outcome, and it can predict early recurrence after surgical resection or Radiofrequency Ablation (RFA) in patients with HCC. However, it requires exogenous contrast agents and is unfriendly to some patients, such as those with poor renal function. In recent years, MRI sequences such as Diffusion-Weighted Imaging (DWI) [12-14], Intra-Voxel Incoherent Motion (IVIM) [15-17], and Diffusion Kurtosis Imaging (DKI) [20], have been shown to improve the assessment of treatment success, thereby improving treatment decision-making and patient outcomes. Traditionally, DWI method is based on the diffusion of water molecules in voxels and follows Gaussian distribution without any restrictions [18]. However, there are complex microstructures in tissues, such as cell membranes and organelles, and the movement of water molecules in biological tissues is restricted and presents a non-Gaussian distribution [19]. IVIM is regarded as an important tool for evaluating neovascularization or microvascular heterogeneity to monitor the therapeutic effect of chemotherapy/radiotherapy [12, 13]. It assumes that water movement in the tissue are divided into perfusion and diffusion, following a bi-exponential model. However, the actual water movement in tissue is more complicated due to the complex environment. Unlike IVIM, the DKI model makes no assumptions about the composition of the dispersion in the tissue. It is a type of diffusion imaging technology that assess the motion of water molecules in tissue as a non-Gaussian distribution and quantify the degree to which the diffusion deviates from the Gaussian distribution. DKI can be used to evaluate the histopathological characteristics and therapeutic efficacy of rectal cancer, glioma and advanced gastric cancer [20-22]. Studies have shown that the increase of MK is significantly correlated with MVI of HCC [23].

If the functional reserve of the liver is insufficient to sustain life, some invasive treatments may have serious adverse effects. Liver function assessment is mainly based on blood parameters or biochemical classification, which lacks imaging basis. At present, some progress has been made in the study of correlation evaluation of liver function by imaging. Some studies have shown that liver dysfunction may occur in some patients after RFA or TACE [24]. Yoon et al. showed that hepatocellular specific contrast agents can be used to quantify liver function25. Multiple studies have shown that dynamic Gd-EOB-DTPA enhanced MRI can be used to evaluate liver function [26, 27]. Some studies have shown that incoherent intravascular diffusion weighted magnetic resonance imaging can be used to evaluate the severity of liver function [28]. Compared with contrast enhancement sequences and IVIM, DKI has the advantage of not requiring exogenous contrast agents and is subject to different model assumptions. Goshima et al. has proved that DKI can be used to assess response to treatment in hypervascular hepatocellular carcinoma [24]. However, there have been little comprehensive studies on TACE treatment response and functional deterioration in HCC by using DKI. This study is aimed to investigate value of DKI imaging in predicting the recurrence and the liver function deterioration of intermediate-stage HCC treated with TACE.

3. Methods

3.1. Patients

This prospective study was approved by the local Ethics Committee. Written informed consent was obtained from all participants before inclusion. From September 2018 to August 2020, 75 patients diagnosed with HCC were initially enrolled and underwent pretreatment DKI examination. The inclusion criteria were as follows: (1) HCC was diagnosed through contrast-enhanced CT and/or MR imaging, serological or pathological examination; (2) intermediate-stage HCC (BCLC stage B according to Barcelona Clinic Liver Cancer staging system 2018 version) [29]; (3) all patients were in accordance with the staging criteria for Eastern Cooperative Oncology Group (ECOG) performance status 0-2; (4) HCC of Child–Pugh class A or B; (5) no surgery, radiotherapy, chemotherapy or other treatments before TACE surgery; (6) no cancer-related symptoms or evidence of vascular invasion or extrahepatic spread. Exclusion criteria: (1) the presence of other diseases that affect the survival of the patients; (2) Child–Pugh grade C; (3) with contraindication for MRI examinations, such as metallic implants, pregnancy, or renal insufficiency. Finally, 63 patients who further underwent TACE were included in the present study, including 28 pathologically confirmed patients and 35 clinically and radiologically diagnosed patients. Pretherapeutic laboratory and clinical data were retrospectively collected in these patients.

3.2. Follow-up and grouping

The patients were followed up for at least six months after TACE, and dCE-MRI or CT of abdomen, tumor markers and biochemical examination of liver function were performed monthly. Thereafter, follow-up was performed every 3 months if necessary.

Tumor response to TACE was evaluated based on the modified Response Evaluation Criteria in Solid Tumors (mRECIST) [30]. The subjects were divided into the recurrence (n=33) and non-recurrence groups (n=30). The non-recurrence group is composed of the patients with Complete Response (CR) and Partial Response (PR), and the recurrence group is composed of the patients with Progressive Disease (PD) and the Stable Disease (SD).

Clinical characteristics were also collected 6 months after TACE. Using these data, the Child-Pugh score after TACE was calculated. Pa-

tients with Child - Pugh Grade C were included in the liver function deterioration group, and patients with Child - Pugh Grade A or B were included in the non-liver function deterioration group. Thirty-three recurrence subjects were divided into liver function deterioration (n=7) and non-liver function deterioration (n=26) groups.

3.3. Procedure of TACE

The Seldinger technique was used to puncture the right femoral artery in all patients, and a 5F catheter was inserted for celiac and hepatic artery angiography in evaluation of the vascular anatomy, tumor staining and the tumor-feeding artery. An emulsion mixture of 30 mg epirubicin, 60 mg cisplatin and 10 ml lipiodol was injected using a 2.7F microcatheter. The TACE procedure was stopped when tumor staining completely disappeared and regional arterial blood flow stopped. The regimen was adjusted depending on liver function, peripheral leukocyte and platelet levels.

3.4. Image Acquisition

All the subjects underwent abdomen MRI on a 3T MR scanner (Discovery MR750W, GE Healthcare, USA) with a 32-channel phased-array torso coil. Before examination, all subjects were forbidden to eat and drink for 6-8 h, and received a training of uniform breathing and breath-holding. The scan ranged from diaphragmatic apex to the lower margin of the liver. We used respiration triggered scanning. Routine abdomen sequences included axial respiratory triggered fat-suppressed fast spin echo (FSE) T2-weighted imaging and 3D Liver Acquisition with Volume Acceleration Flex (3D LAVA Flex) sequences with breath-hold. After conventional MRI scanning, a single-shot echo-planar imaging (SS-EPI) sequence was used to acquire two-dimensional axial DKI images. The DKI data were acquired along 30 directions, with b values of 0, 1000, and 2000 s/mm2. A detailed description of the MR imaging parameters is shown in Table 1.

Table 1: Details of MRI Parameters

Parameters	T1-weighted Imaging	T2-weighted Imaging	DKI
Sequences	LAVA flex	FSE T2WI	SS-EPI
Repetition time/echo time (ms)	4.3/1.6	10,000/70	2500/58.9
Flip angle (degrees)	14	110	90
Field of view (mm^2)	360×324	360×360	360×280
Matrix (frequency × phase)	260×210	320×320	128×128
Number of excitations	1	1.5	2
Slice thickness (mm)	4.0	4.0	5.0
Slice gap (mm)	0	0.5	1.0
No. of slices	24	24	24

LAVA = liver acquisition with volume acceleration; FSE = fast spin-echo; SS-EPI = single Shot Echo Planar Imaging, PI = echo-planar imaging; N/A = not applicable

3.5. Data Postprocessing

After liver MR scanning, the imaging data were transferred to the GE AW4.6 workstations (Advantage workstation 4.6, GE Healthcare, Milwaukee, WI, USA) for post-processing. First, tumor borders were drawn on the original images of DKI sequences based on TIWI and T2WI. Subsequently, regions of interest (ROIs) with the same size (~100 mm_2) were manually delineated three times in the solid part of the tumor, peritumoral, and normal tissues by xx experienced radiologists, carefully avoiding large blood vessels, calcification, cystic changes, and hemorrhage. Finally, the ROIs in the original DKI images were automatically copied to the pseudo-colored maps to obtain the values of Mean Diffusivity (MD), Mean Kurtosis (MK) and Fractional Anisotropy (FA).

3.6. Statistical Analysis

Statistical analyses were performed on SPSS version 26.0 (IBM Corporation, Armonk, NY, USA) and MedCalc version 19.2.0 (MedCalc, Mariakerke, Belgium) software. Quantitative variables are expressed as mean ± standard deviation (SD), and group differences of quantitative variables were analyzed by using Analysis of Variance (ANOVA) or independent t-test. The inter-observer agreement for DKI measurements was assessed by calculating Interclass Correlation Coefficient (ICC) (<0.40, poor; 0.40-0.59, fair; 0.60-0.74, good; and 0.75-1.00, excellent). Univariate and multivariate logistic regression analyses were used to identify independent factors of tumor response to TACE and postoperative liver hepatic decompensation. A prediction model was derived from the multivariate logistic regression analysis results. Factors with a $P < 0.05$ at univariate analyses were included in the multivariate model. Receiver Operating Characteristic (ROC) analyses were performed to evaluate the predictive performance of the model and other significant parameters in tumor response to TACE and postoperative liver hepatic decompensation. $P < 0.05$ was considered to indicate a significant difference.

4. Results

4.1. Demographics and Clinical Characteristics

Sixty-three patients with HCC (56 males and 7 females; mean age 57.2 ±13.6 years; range 31-85years) were included in our study for final data analysis. Baseline characteristics of the patients are summarized in Table 2.

Table 2: Baseline Characteristics of All the Patients with HCC by TACE

Variables	All patients（n=63）	recurrence groups（n=33）	non-recurrence groups（n=30）	P value
Gender (male/female)	56/7	29/4	27/3	0.292
Age (y)[a]	57.2±13.6	56.0±14.5	58.5±12.7	0.488
Liver cirrhosis (yes/no)	48/15	26/7	22/8	0.618
HBV (yes/no)	52/11	28/5	24/6	0.619
Child–Pugh (A/B)	33/30	15/18	18/12	0.127
Tumor number (1/2/≥3)	20/20/23	10/12/11	10/8/12	0.680
Serum AFP levels (ng/mL)[a]	2073±5078	2637±6349	1451±3145	0.359
Tumor size (cm)[a]	5.5±2.8	4.6±2.2	6.5±3.1	0.006

[a]Values are expressed as mean±standard deviation

HCC, hepatocellular carcinoma; TACE, transarterial chemoembolization; HBV, hepatitis B virus; AFP, alpha-fetoprotein.

4.2. Consistency Test

The ICC of the diffusion metrics between two readers showed good or excellent consistency in the tumor tissue (0.915 for MK, 0.856 for MD, 0.754 for FA), in the peritumoral tissue (0.861 for MK, 0.869 for MD, 0.856 for FA), and in the normal tissue (0.852 for MK, 0.816 for MD, 0.759 for FA).

4.3. Comparisons of DKI Parameters Between the Recurrence and Non-Recurrence Groups

There were significant differences in MK (P = 0.002) and MD (P < 0.001) values among the tumor, peritumoral tissue, and normal tissue. No significant differences were shown in FA (P = 0.547) among these tissues. Details are shwon in Table 3. Figures 1 and 2 show pretreatment DKI images of patients with tumor response and non-response after TACE, respectively.

In the tumor tissues, the MK value of the recurrence group (0.820 ± 0.090) was significantly higher than that of the non-recurrence group (0.653 ± 0.108) (P < 0.001). The MD value of the recurrence group ([1.334±0.217]×10-^{3}mm^{2} /s) was significantly lower than that of the non-recurrence group ([1.473±0.293]×10-^{3}mm^{2}/s) (P = 0.036). There were no significant differences in the FA (P = 0.098) between the two groups. (Figure 3A)

In the peritumoral tissues, the MK value of the recurrence group (0.716±0.103) was significantly higher than that of the non-recurrence group (0.648±0.082) (P = 0.006). There were no significant differences in the MD and FA values between the two groups (P = 0.238 and P = 0.303, respectively). (Figure 3B)

Table 3: Comparison of DKI Parameters Between Tissue Types

Parameters	TT	PT	NT	P	P (TT vs.PT)	P (TT vs. NT)	P (PT vs. NT)
MK	0.741±0.129	0.684±0.099	0.683±0.079	0.002	0.002	0.002	0.992
MD(×10^{-3}mm^{2}/s)	1.400±0.263	1.509±0.192	1.645±0.329	<0.001	0.024	<0.001	0.005
FA	0.365±0.203	0.349±0.128	0.381±0.156	0.547	-	-	-

All quantitative data are expressed as mean±standard deviation. P < 0.05 calculated using one-way analysis of variance (ANOVA) and post hoc analysis.DKI diffusion kurtosis imaging, MK mean kurtosis, MD mean diffusivity,FA fractional anisotropy.TT = tumor tissue; PT = peritumoral tissue; NT = normal tissue.

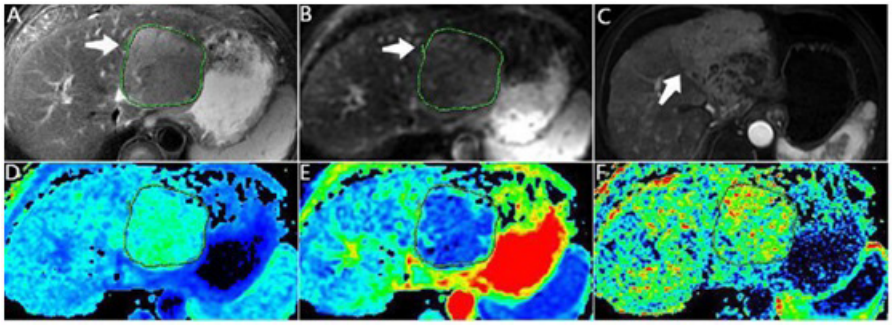

Figure 1: Images in a 56-year-old man patient with HCC who showed tumor response to TACE.

(A) T2-weighted image, (B) Diffusion-weighted image, (C) DCE images of tumor recurrence after TACE, (D) Mean kurtosis pseudo-colored map, (E) Mean diffusivity pseudo-colored map, (F) fractional anisotropy image

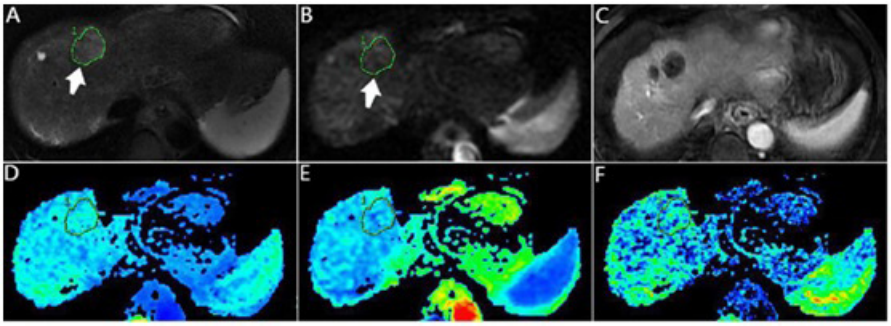

Figure 2: Images in a 68-year-old man patient with HCC who did not show tumor response to TACE.

(A) T2-weighted image, (B) Diffusion-weighted image, (C) DCE images of tumor non-recurrence after TACE, (D) Mean kurtosis pseudo-colored map, (E) Mean diffusivity pseudo-colored map, (F) fractional anisotropy image

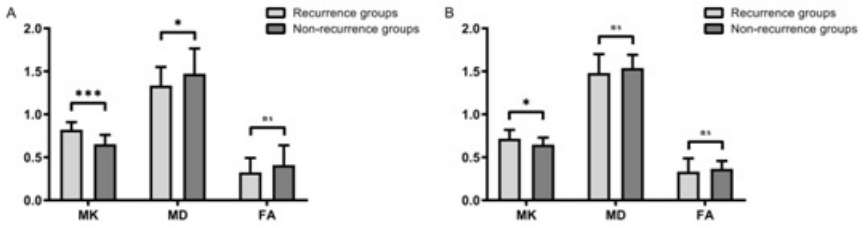

Figure 3: Column and scatter plot diagrams show the differences of the MK, MD and FA values between the recurrence group and the non-recurrence groups in tumor tissues(A) and peritumor tissues(B).

*P < 0. 05 ; **P < 0.01; ***P < 0.001; ns:not significant.

4.4. Risk Factors for Predicting Tumor Response

As shown in Table 4, univariate analysis identified that the tumor size (P = 0.010), MK and MD of the tumor (P <0.001 and P = 0.043, respectively), and MK of the peritumoral tissue (P = 0.010) were independent predictors of tumor response to TACE. Under multivariate analysis, tumor size (P = 0.004), MK of tumor tissue (P <0.001) were identified as independent predictors of tumor response to TACE. Then, the tumor size and tumor MK were combined in a multiparametric predictive model, which was expressed as logit (P) =-3.764+0.061×tumor size-3.052×MK. The AUC of tumor size and tumor MK were 0.682 and 0.861, respectively, as shown in Figure 4 and listed in Table 5. The AUC of prediction model was 0.940.

Table 4: Univariate and Multivariate Analyses of Pretreatment Prediction for Tumor Response to TACE

Variable	Univariate analysis		Multivariate analysis	
	Odds Ratio (95% CI)	P value	Odds Ratio (95% CI)	P value
Age	1.013(0.977-1.051)	0.481	…	…
Gender	0.400(0.072-2.237)	0.297	…	…
HBsAg	1.000 (1.000–1.000)	0.369	…	…
Cirrhosis	1.351(0.422-4.319)	0.612	…	…
AFP	1.000 (1.000–1.000)	0.369	…	…
Tumor number	0.904(0.564-1.449)	0.675	...	…
Tumor size	1.028(1.007-1.049)	0.01	1.060(1.019-1.102)	0.004
Tumor tissue				
MK	0.112(0.038-0.330)	0	0.068(0.016-0.282)	0
MD(×10^{-3} mm^2/s)	1.790(1.018-3.145)	0.043	1.735(0.610-4.934)	0.301
FA	9.938(0.582-169.669)	0.113	…	…
Peritumoral tissue				
MK	0.440(0.235-0.824)	0.01	0.536(0.170-1.694)	0.288
MD(×10^{-3} mm^2/s)	5.179(0.331-81.035)	0.241	…	…
FA	8.887(0.132-597.121)	0.309	…	…

CI = confidence interval; AFP = alpha-fetoprotein; HbsAg: hepatitis B virus surface antigen.

Table 5: Predictive Performance for Identifying Tumor Response to TACE

Variable	AUC	P value	Sensitivity (%)	Specificity (%)	Youden's index
Tumor size (cm)	0.682	0.013	81.8	50	0.318
MK	0.861	<0.001	100	60	0.6
The prediction model	0.940	<0.001	90.9	93.3	0.842

P < 0.05.AUC = areas under the receiver operating characteristic curve.

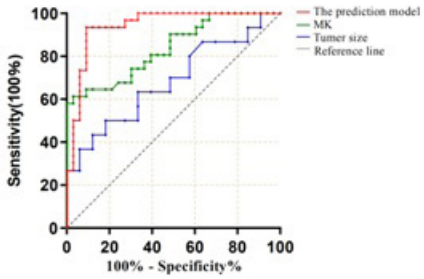

Figure 4: ROC curves for predicting tumor response to TACE.

5. Comparison in DKI Parameters Between the Liver Function Deterioration and Non-liver

5.1. Function Deterioration Groups

Liver function were assessed on the normal liver tissue. Of the 33 recurrence patients, 7 deteriorated to Child-Pugh C (Table 6). There were significant differences in tumor size (P = 0.014), MK (P = 0.001), MD (P = 0.024) between the groups with liver function deterioration and non-liver function deterioration.

As shown in Table 7, univariate logistic regression analysis for predicting the deterioration of the liver function showed that the tumor size (P = 0.031) and MK value (P = 0.018) were statistically significant prognostic factors. In multivariate analysis, only MK (P = 0.030) was identified as independent predictors for deterioration in the liver function. Tumor size (P = 0.061) tended to be an independent predictors. This may be due to the small sample size of this study. The predictive model with the independent factor MK has an AUC of 0.832 as shown in Figure 5.

Table 6: Baseline Characteristics of Liver Function Deterioration group and non-deterioration group in recurrence Patients after TACE

Variables	liver function deterioration groups（n=7）	non-liver function deterioration groups（n=26）	P value
Gender (male/female)	5/2	23/3	0.279
Age (y)	49.9±14.0	57.7±14.5	0.208
Liver cirrhosis (yes/no)	6/1	20/6	0.605
HBV (yes/no)	5/2	23/3	0.945
Child–Pugh (A/B)	4/3	10/16	0.085
Tumor number (1/2/≥3)	2/3/2	8/9/9	0.604
Serum AFP levels (ng/mL)	1096.8±1555.5	3052.5±7083.4	0478
Tumor size (cm)	2.8±1.2	5.0±2.0	0.014
MK	0.775±0.094	0.654±0.069	0.001
MD	1.446±0.047	1.689±0.265	0.024

Table 7: Univariate and Multivariate Analyses of Liver Function Deterioration after TACE

Variable	Univariate analysis		Multivariate analysis	
	Odds Ratio (95% CI)	P value	Odds Ratio (95% CI)	P value
Age	0.962(0.904-1.022)	0.208	…	…
Gender	3.067(0.401-23.440)	0.280	…	…
HBsAg	0.917(0.086–9.805)	0.943	…	…
Cirrhosis	1.680(0.249-11.322)	0.594	…	…
AFP	1.000 (1.000–1.000)	0.502	…	…
Tumor number	0.805(0.364-1.782)	0.593	…	…
Tumor size	0.933(0.875-0.944)	0.031	0.913(0.831-1.004)	0.061
MK	7.666(1.408-41.747)	0.018	10.779(1.218-95.407)	0.033
MD($\times 10^{-3}$ mm^2/s)	0.000(0.000-1.522)	0.057	…	…
FA	1.216(0.551-2.683)	0.628	…	…

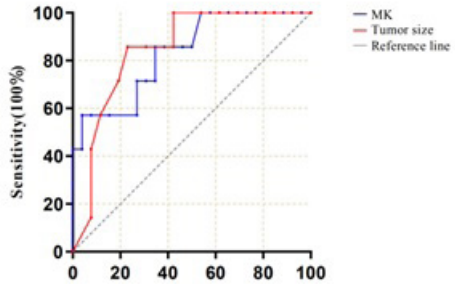

Figure 5: ROC curves for prediction of liver function deterioration.
The AUC of MK and tumor size are 0.832 and 0.846, respectively.

6. Discussion

Our results suggest that DKI imaging is a non-invasive method for predicting early recurrence and liver function deterioration of HCC. Logistic regression analysis showed that the tumor size and tumor MK were independent predictors of HCC response to TACE. MK value can also be used as a predictor of liver function deterioration in recurrence patients after TACE. In this study, we found that the MK value of peritumor tissue and normal tissue were significantly lower than that of the tumor tissues, and the MD value progressively decreased from that in normal tissue to that of tumor tissue. Feely et al. have shown that systemic DKI could better reflect the microstructure of tissue than DWI [31]. Tan et al. have reported that the MK value in peritumoral tissue was significantly higher in the high-grade astrocytomas than in the low-grade astrocytomas [32]. Di T et al. have shown that the MK value was significantly different in tumor tissues, peri-tumor tissues and benign tissues of prostate, indicating that the characteristics of peri-tumor tissues were different from other tissues [33]. In addition, in post-mortem analysis, there were significant differences in MD values among the three tissues. Some studies have shown that MD value is helpful in differentiating normal pancreatic parenchyma, peri-lesion inflammation and pancreatic tumor [34]. This may be due to the release of inflammatory factors [35-37], (IL-17, CXCL8, 12, 14, etc.), increased vascular permeability, and endothelial cell migration, leading to extravasation of extracellular fluid around the tumor tissue. On the other hand, malignant tumors often have microvascular infiltration, and tumor cells spread to the peri-tumor tissues, resulting in a more complex and irregular tumor microenvironment. The accumulation of large numbers of neutrophils can act as a hub for the proinflammatory response and angiogenesis in the tumor milieu.

Our results revealed that the MK value were significantly different between the recurrence and non-recurrence groups in both tumor and peritumoral tissues. Yu et al. demonstrated the feasibility of DKI in evaluating response to neoadjuvant radiotherapy for rectal cancer [38]. Guo et al. reported that the difference of MK value between the good response group in the treatment of malignant bone tumors and poor response group was significant [39]. They believe that the relapsing group had more hypoxic and acidic environments, leading to tissue necrosis and fibrosis. Our study is consistent with the results that MK value can predict the early stage of neoadjuvant chemotherapy for locally advanced gastric cancer [40] and radiotherapy for nasopharyngeal cancer [41]. Compared with the non-recurrent group, the recurrent group may have more tumor cells, larger nuclei, more obvious cellular heterogeneity and more interstitial blood vessels, leading to more complex microstructure and heterogeneity. Previous studies [42, 43] have shown that the N/C ratio of tumor cells is positively correlated with MK, which may be due to the decrease of extracellular space and limited motion of water molecules with the increase of tumor cell proliferation and tumor microstructure complexity. Therefore, the MK value of the recurrence group was significantly higher than that of the non-recurrence groups. In addition, some studies have shown that MD value can reflect the changes of tumor biomarker expression and proliferation activity in vivo, which was inconsistent with the results of this study, possibly due to the inconsistency of the population or insufficient sample size [23, 27].

Multivariable logistics regression model analysis showed that tumor MK and tumor size were independent predictor of tumor response. An integrated model derived from these variables reached an AUC of 0.940 for prediction of the risk of tumor recurrence. The prediction model that uses preoperative MR imaging has the potential to preoperatively identify high-risk patients, and assist in the selection of alternative treatments.

Most HCC patients have limited normal hepatic function, and their prognosis partially depends on the level of hepatic functional reserve. Some patients with Child-pugh Grade C can be improved to Child-pugh Grade B or Grade A after large amount of albumin supplementation and diuretic regression of ascites, which is easy to cause postoperative liver function decompression [21]. A study has shown that MK increased with fibrosis levels [44]. Anderson et al. have used rat models to study the imaging changes in human liver fibrosis, and found that MK value derived from DKI model strongly correlates with the degrees of hepatic fibrosis when compared with either the stretched exponential or monoexponential models [45]. Our study has been conducted to identify the risk biomarker for liver function deterioration after TACE. It shows that MK value has a high predictive value for patients who are expected to be refractory to TACE and have a high likelihood of a deterioration in liver function. This may be due to the high degree of liver fibrosis and liver function grade in the liver function deterioration group after surgery. The swelling of liver cells and inflammatory cell infiltration, the deposition of collagen molecules, glycosaminoglycan and proteoglycan in the extracellular space leads to the narrowing of the extracellular space and the limitation of the diffusion in the liver. This finding helps to provide patients with rapid conversion therapy, such as sorafenib and recolafenib.46 Although tumor size was significant in the univariate analysis, the significance was excluded in the multivariate analysis, which is different from the results of Huo et al [47]. But we have seen the independent tendency of tumor size. This may be due to the small sample size of this study.

First, the sample size should be enlarged. A larger sample size is needed to verify the results of this study in clinical practice. Second, the follow-up time may be short, and different time points need to be set to further study the relationship between DKI and treatment response. Third, due to small sample size we only compared the liver function deterioration group (Child C) and the non-liver function deterioration group (Child A+Child B), and did not compare the postoperative Child A with the postoperative Child B groups. Fourth, further study on the correlation between tumor recurrence and liver deterioration at different follow-up time points are needed.

Tumor size and pre-treatment MK value derived from DKI were independent factors for predicting TACE response of intermediate-stage HCC. The combined prediction model has the potential to preoperatively identify high-risk patients, and assist in the selection of alternative treatments. In addition, MK value can also be used as a risk factor for liver function deterioration after TACE. This helps to select patients who are suitable for TACE treatment, and provide early warning to patients at risk of liver function deterioration after surgery to consider switching to other treatments.

References

1. Yang D, She H, Wang X, Yang Z, Wang Z. Diagnostic accuracy of quantitative diffusion parameters in the pathological grading of hepatocellular carcinoma: A meta-analysis. J Magn Reson Imaging. 2020; 51(5): 1581-93.
2. Park Y, Kim BK, Park JY, et al. Feasibility of dynamic risk assessment for patients with repeated trans-arterial chemoembolization for hepatocellular carcinoma. BMC Cancer. 2019; 19(1): 363.
3. Chen RX, Gan YH, Ge NL, et al. A new prediction model for prognosis of patients with intermediate-stage HCC after conventional transarterial chemoembolization: an internally validated study. J Cancer. 2019; 10(26): 6535-42.
4. Soysal SD, Tzankov A, Muenst SE. Role of the Tumor Microenvironment in Breast Cancer. Pathobiology. 2015; 82(3-4): 142-52.
5. Ippolito D, Trattenero C, Talei Franzesi C, et al. Dynamic Contrast-Enhanced Magnetic Resonance Imaging With Gadolinium Ethoxybenzyl Diethylenetriamine Pentaacetic Acid for Quantitative Assessment of Vascular Effects on Hepatocellular-Carcinoma Lesions Treated by Transarterial Chemoembolization or Radiofrequency Ablation. J Comput Assist Tomogr. 2016; 40(5): 692-700.
6. Hunt SJ, Yu W, Weintraub J, Prince MR, Kothary N. Radiologic monitoring of hepatocellular carcinoma tumor viability after transhepatic arterial chemoembolization: estimating the accuracy of contrast-enhanced cross-sectional imaging with histopathologic correlation. J Vasc Interv Radiol. 2009; 20(1): 30-8.
7. Kubota K, Hisa N, Nishikawa T, et al. Evaluation of hepatocellular carcinoma after treatment with transcatheter arterial chemoembolization: comparison of Lipiodol-CT, power Doppler sonography, and dynamic MRI. Abdom Imaging. 2001; 26(2): 184-90.
8. Lee S, Kim SH, Lee JE, Sinn DH, Park CK. Preoperative gadoxetic acid-enhanced MRI for predicting microvascular invasion in patients with single hepatocellular carcinoma. J Hepatol. 2017; 67(3): 526-34.
9. Lee S, Kang TW, Song KD, et al. Effect of Microvascular Invasion Risk on Early Recurrence of Hepatocellular Carcinoma After Surgery and Radiofrequency Ablation. Ann Surg. 2021; 273(3): 564-71.
10. Romanzi A, Ariizumi S, Kotera Y, et al. Hepatocellular carcinoma with a non-smooth tumor margin on hepatobiliary-phase gadoxetic acid disodium-enhanced magnetic resonance imaging. Is sectionectomy the suitable treatment?. J Hepatobiliary Pancreat Sci. 2020; 27(12): 922-30.
11. Lee S, Kim KW, Jeong WK, et al. Gadoxetic acid-enhanced MRI as a predictor of recurrence of HCC after liver transplantation. Eur Radiol. 2020; 30(2): 987-95.
12. Yu JS, Kim JH, Chung JJ, Kim KW. Added value of diffusion-weighted imaging in the MRI assessment of perilesional tumor recurrence after chemoembolization of hepatocellular carcinomas. J Magn Reson Imaging. 2009; 30(1): 153-60.
13. Wu XM, Wang JF, Ji JS, Chen MG, Song JG. Evaluation of efficacy of transcatheter arterial chemoembolization for hepatocellular carcinoma using magnetic resonance diffusion-weighted imaging. Onco Targets Ther. 2017; 10: 1637-43.
14. Muhi A, Ichikawa T, Motosugi U, et al. Diffusion-weighted imaging of hepatocellular carcinoma for predicting early recurrence and survival after hepatectomy. Hepatol Int. 2013; 7(2): 662-8.
15. Le Bihan D. What can we see with IVIM MRI?. Neuroimage. 2019; 187: 56-67.
16. Park YS, Lee CH, Kim JH, et al. Using intravoxel incoherent motion (IVIM) MR imaging to predict lipiodol uptake in patients with hepatocellular carcinoma following transcatheter arterial chemoembolization: a preliminary result. Magn Reson Imaging. 2014; 32(6): 638-46.
17. Wei Y, Huang Z, Tang H, et al. IVIM improves preoperative assessment of microvascular invasion in HCC. Eur Radiol. 2019; 29(10): 5403-14.
18. Le Bihan D, Breton E, Lallemand D, Grenier P, Cabanis E, Laval-Jeantet M. MR imaging of intravoxel incoherent motions: application to diffusion and perfusion in neurologic disorders. Radiology. 1986; 161(2): 401-7.
19. Jensen JH, Helpern JA. MRI quantification of non-Gaussian water diffusion by kurtosis analysis. NMR Biomed. 2010; 23(7): 698-710.
20. Yu J, Xu Q, Song JC, et al. The value of diffusion kurtosis magnetic resonance imaging for assessing treatment response of neoadjuvant chemoradiotherapy in locally advanced rectal cancer. Eur Radiol. 2017; 27(5): 1848-57.
21. Bai Y, Lin Y, Tian J, et al. Grading of Gliomas by Using Monoexponential, Biexponential, and Stretched Exponential Diffusion-weighted MR Imaging and Diffusion Kurtosis MR Imaging. Radiology. 2016; 278(2): 496-504.
22. Fu J, Tang L, Li ZY, et al. Diffusion kurtosis imaging in the prediction of poor responses of locally advanced gastric cancer to neoadjuvant chemotherapy. Eur J Radiol. 2020; 128: 108974.
23. Wang WT, Yang L, Yang ZX, et al. Assessment of Microvascular Invasion of Hepatocellular Carcinoma with Diffusion Kurtosis Imaging. Radiology. 2018; 286(2): 571-80.
24. Goshima S, Kanematsu M, Noda Y, Kondo H, Watanabe H, Bae KT. Diffusion kurtosis imaging to assess response to treatment in hypervascular hepatocellular carcinoma. AJR Am J Roentgenol. 2015; 204(5): W543-W549.
25. Yoon JH, Lee JM, Kang HJ, et al. Quantitative Assessment of Liver Function by Using Gadoxetic Acid-enhanced MRI: Hepatocyte Uptake Ratio. Radiology. 2019; 290(1):125-33.
26. Xie S, Sun Y, Wang L, Yang Z, Luo J, Wang W. Assessment of liver function and liver fibrosis with dynamic Gd-EOB-DTPA-enhanced MRI. Acad Radiol. 2015; 22(4): 460-6.
27. Haimerl M, Verloh N, Zeman F, et al. Gd-EOB-DTPA-enhanced MRI for evaluation of liver function: Comparison between signal-intensity-based indices and T1 relaxometry. Sci Rep. 2017; 7: 43347.
28. Zhang J, Guo Y, Tan X, et al. MRI-based estimation of liver function by intravoxel incoherent motion diffusion-weighted imaging. Magn Reson Imaging. 2016; 34(8): 1220-5.

29. Zhou J, Sun H, Wang Z, et al. Guidelines for the Diagnosis and Treatment of Hepatocellular Carcinoma (2019 Edition). Liver Cancer. 2020; 9(6): 682-720.
30. Lencioni R, Llovet JM. Modified RECIST (mRECIST) assessment for hepatocellular carcinoma. Semin Liver Dis. 2010; 30(1): 52-60.
31. Filli L, Wurnig M, Nanz D, Luechinger R, Kenkel D, Boss A. Whole-body diffusion kurtosis imaging: initial experience on non-Gaussian diffusion in various organs. Invest Radiol. 2014; 49(12): 773-8.
32. Tan Y, Zhang H, Zhao RF, Wang XC, Qin JB, Wu XF. Comparison of the values of MRI diffusion kurtosis imaging and diffusion tensor imaging in cerebral astrocytoma grading and their association with aquaporin-4. Neurol India. 2016; 64(2): 265-72.
33. Di Trani MG, Nezzo M, Caporale AS, et al. Performance of Diffusion Kurtosis Imaging Versus Diffusion Tensor Imaging in Discriminating Between Benign Tissue, Low and High Gleason Grade Prostate Cancer. Acad Radiol. 2019; 26(10): 1328-37.
34. Granata V, Fusco R, Sansone M, et al. Magnetic resonance imaging in the assessment of pancreatic cancer with quantitative parameter extraction by means of dynamic contrast-enhanced magnetic resonance imaging, diffusion kurtosis imaging and intravoxel incoherent motion diffusion-weighted imaging. Therap Adv Gastroenterol. 2020; 13: 1756284819885052.
35. Panzironi G, Moffa G, Galati F, Marzocca F, Rizzo V, Pediconi F. Peritumoral edema as a biomarker of the aggressiveness of breast cancer: results of a retrospective study on a 3 T scanner. Breast Cancer Res Treat. 2020; 181(1): 53-60.
36. Ren Y, Poon RT, Tsui HT, et al. Interleukin-8 serum levels in patients with hepatocellular carcinoma: correlations with clinicopathological features and prognosis. Clin Cancer Res. 2003; 9(16 Pt 1): 5996-6001.
37. Orimo A, Gupta PB, Sgroi DC, et al. Stromal fibroblasts present in invasive human breast carcinomas promote tumor growth and angiogenesis through elevated SDF-1/CXCL12 secretion. Cell. 2005; 121(3): 335-48.
38. Yu J, Xu Q, Song JC, et al. The value of diffusion kurtosis magnetic resonance imaging for assessing treatment response of neoadjuvant chemoradiotherapy in locally advanced rectal cancer. Eur Radiol. 2017; 27(5): 1848-57.
39. Guo J, Dong C, Wu Z, et al. Diffusion kurtosis imaging assessment of the response to radiotherapy in a VX2 bone tumor model: an animal study [published online ahead of print, 2021 Feb 3]. Acta Radiol. 2021; 63(2): 182-191.
40. Le Bihan D, Breton E, Lallemand D, Grenier P, Cabanis E, Laval-Jeantet M. MR imaging of intravoxel incoherent motions: application to diffusion and perfusion in neurologic disorders. Radiology. 1986; 161(2): 401-7.
41. Huang WY, Li MM, Lin SM, et al. In Vivo Imaging Markers for Prediction of Radiotherapy Response in Patients with Nasopharyngeal Carcinoma: RESOLVE DWI versus DKI. Sci Rep. 2018; 8(1): 15861.
42. Dai Y, Yao Q, Wu G, et al. Characterization of clear cell renal cell carcinoma with diffusion kurtosis imaging: correlation between diffusion kurtosis parameters and tumor cellularity. NMR Biomed. 2016; 29(7): 873-81.
43. Haopeng P, Xuefei D, Yan R, et al. Diffusion kurtosis imaging differs between primary central nervous system lymphoma and high-grade glioma and is correlated with the diverse nuclear-to-cytoplasmic ratio: a histopathologic, biopsy-based study. Eur Radiol. 2020; 30(4): 2125-37.
44. Hu G, Liang W, Wu M, et al. Staging of rat liver fibrosis using mono-exponential, stretched exponential and diffusion kurtosis models with diffusion weighted imaging- magnetic resonance. Oncotarget. 2017; 9(2): 2357-66.
45. Anderson SW, Barry B, Soto J, Ozonoff A, O'Brien M, Jara H. Characterizing non-gaussian, high b-value diffusion in liver fibrosis: Stretched exponential and diffusional kurtosis modeling. J Magn Reson Imaging. 2014; 39(4): 827-34.
46. Kudo M. A New Era of Systemic Therapy for Hepatocellular Carcinoma with Regorafenib and Lenvatinib. Liver Cancer. 2017; 6(3): 177-184.
47. Huo TI, Lui WY, Wu JC, et al. Deterioration of hepatic functional reserve in patients with hepatocellular carcinoma after resection: incidence, risk factors, and association with intrahepatic tumor recurrence. World J Surg. 2004; 28(3): 258-62.